machines

MDPI

Article

Research and Mechanism Design Analysis of Leg Lifting Device Based on Human Body Stretching

Ruijie Gu, Jiameng Gao, Shuaifeng Zhao * and Hao Xing

School of Mechatronics Engineering, Henan University of Science and Technology, Luoyang 471003, China; iapte@haust.edu.cn (R.G.)
* Correspondence: zsf588@haust.edu.cn

Abstract: Leg stretching devices are one of the main instruments used to improve human function. To solve the limitations of existing leg stretching products, such as single function and low degree of coincidence, a leg stretching device satisfying ergonomics was studied in this paper. Firstly, the Box–Behnken Design (BBD) response surface methodology was applied to establish a regression model for leg force. Secondly, a motion analysis was conducted on the leg lifting mechanism using analytical methods, and the model data were coupled by Creo Parametric and Automatic Dynamic Analysis of Mechanical System (ADAMS) 2019 software to develop the kinematic model. Then, the motion characteristics during the whole process were studied, and the motion parameter curves were obtained. Next, ABAQUS 2022 software was employed to create the finite element simulation model of the leg lifting device, and key component strength was also analyzed. Finally, a prototype of the device was made and experimentally validated with leg lifting. The results show that in the case of different heights and weights, the lifting angle of the human leg has a significant effect on the force state during the leg lifting process. When the leg is lifted 0–30°, the force on the leg is small. As the leg lifting angle increases, the force on the leg also increases. In the process of leg lifting, the angular velocity and angular acceleration of the leg lifting mechanism change more gently, and there is no obvious mutation. The maximum stress of the driving rod is 102.5 MPa, the maximum stress of the lifting rod is 88.12 MPa, and the maximum stress of the leg placing plate is 40.5 MPa, all of which meet the strength requirements and provide a reference for the research of the human leg stretching device.

Keywords: leg stretching; kinematic analysis; response surface methodology; strength analysis

check for updates

Academic Editor: Jose Machado

Received: 1 December 2024
Revised: 10 January 2025
Accepted: 21 January 2025
Published: 22 January 2025

Citation: Gu, R.; Gao, J.; Zhao, S.; Xing, H. Research and Mechanism Design Analysis of Leg Lifting Device Based on Human Body Stretching. *Machines* **2025**, *13*, 78. https://doi.org/10.3390/machines13020078

Copyright: © 2025 by the authors. Licensee MDPI, Basel, Switzerland. This article is an open access article distributed under the terms and conditions of the Creative Commons Attribution (CC BY) license (https://creativecommons.org/licenses/by/4.0/).

1. Introduction

According to a World Health Organization report, over 2 million people die each year due to excessive physical exertion [1]. Mechanical devices for controlled stretching exercises have become one of the most effective methods for relieving both mental and physical stress [2–5]. To reduce physical muscle fatigue, an increasing number of researchers are focusing on the development of human muscle and skeletal stretching devices.

A large number of scholars have conducted extensive research on the movement characteristics of human body stretching devices. For example, Mukul et al. [6] studied the Rewalk lower limb exoskeleton mechanism, Neuhaus et al. [7] proposed the Mina lower limb rehabilitation mechanism, and Li et al. [8] proposed a lower limb robot. These robots exhibit good bionic characteristics, significantly enhancing the effectiveness of human rehabilitation training [9]. ANYexo2.0 [10], with its unique motion structure and bionic shoulder

coupling control, enables users to train a wide range of everyday upper limb movements and interact with real objects. Pang and Yan et al. [11,12] designed an upper limb rehabilitation robot and validated the design's feasibility through kinematic analysis, offering valuable insights for research in human rehabilitation robotics. Fang and Zou et al. [13,14] studied a walking rehabilitation training robot, which not only improved reliability through the use of a suspension device but also proposed a coordinated control method, offering valuable insights for further research on this type of robot. Kumar et al. [15] developed a two-arm rehabilitation mechanism mounted on a wheelchair, which helps reduce the weight borne by the human body. Shi et al. [16] proposed a lower limb rehabilitation training robot based on human bionics, verifying the mechanism's feasibility through theoretical analysis and ADAMS 2017 simulation software, thus laying the foundation for prototype development. Ceccarelli et al. [17] proposed a portable design for an arm movement device, which is easy to assemble and operate. KwangWoo et al. [18] used motion capture devices to estimate the corresponding motion data, which was reflected in the design of a shoulder wearable device. Russo et al. [19] proposed a wearable device for ankle joint movement and analyzed the design of the mechanism using kinematics and static models to verify the feasibility of the design. Based on varying user needs for lower limb training, Diana et al. [20] proposed a lower limb exoskeleton robot designed for gait rehabilitation, effectively achieving the desired rehabilitation outcomes for human lower limbs. Researchers in Korea designed and manufactured the LokoHelp lower extremity stretching and rehabilitation training mechanism, which consists of a treadmill, a leg orthopedic device, and a suspension weight reduction system, thereby enhancing the device's functionality [21]. Researchers in Japan developed the HAL lower extremity stretching rehabilitation training mechanism, capable of performing a series of simple movements to meet a person's daily needs [22].

Despite extensive research by numerous scholars on the design, manufacture, and analysis of human-body-related devices, these devices still face challenges such as complex structures, excessive weight, and a lack of relevant human body testing, which prevent them from fully meeting the movement requirements of the human body.

Therefore, this paper first studies the tensile action of human leg lifting and uses the response surface method to study that the most influential force on the human leg lifting process is the leg lifting angle, and at 0–30°, the leg is less stressed. When lifting 90°, the leg is the most stressed. Furthermore, a leg lifting mechanism that meets the actual stretching requirements of human legs is designed. Based on the experimental results of leg force, the motion and strength of the mechanism are analyzed, and the motion parameter curve and the strength of the key components of the leg lifting mechanism are obtained. It is concluded that the motion range of the leg lifting device can meet the tensile demand, the angular velocity and angular acceleration change are relatively stable, and the motion performance is good. The strength of the leg lifting mechanism meets the requirements. It provides a reference for the research of human-leg-related devices.

2. Methods

2.1. Stages for Implementing the Leg Stretching Prototype

2.1.1. Stage 1: Requirements for Human Leg Lifting Action

To make the design of the human leg lifting action mechanism more in line with the actual working conditions of stretching, this section determines the overall test program of the leg lifting action mechanism through the study of the human leg lifting process of the movement state, characteristics, and the actual demand for stretching, and the force changes of people with different heights and weights when their legs are lifted at different angles are obtained. It lays a foundation for the design, model establishment, and strength

analysis of the driving rod and lifting rod of the leg lifting mechanism. The schematic diagram of human leg lifting action is shown in Figure 1.

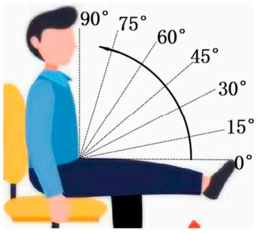

Figure 1. Schematic diagram of human leg lifting.

2.1.2. Stage 2: Design of Leg Lifting Action Mechanism

The leg lifting mechanism designed in this paper utilizes a decelerating motor to drive a connecting rod. The motor drives the driving rod, which in turn drives the lifting rod, lifting the leg placing plate. This mechanism enables the lifting and landing actions of the plate. A schematic diagram of the lifting mechanism is shown in Figure 2, where Figure 2a represents the horizontal state and Figure 2b represents the vertical state of the lifting mechanism.

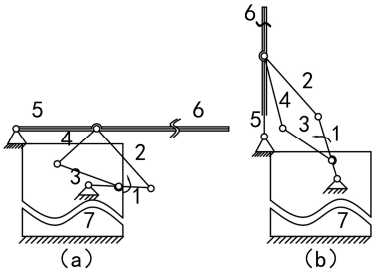

Figure 2. Schematic of the motion of the lifting mechanism: 1. drive rod; 2. lift rod; 3. drive auxiliary rod; 4. lift auxiliary rod; 5. leg placing plate; 6. slide plate; 7. bracket; (**a**) horizontal state; (**b**) vertical state.

The leg lifting mechanism consists of a bracket, a driving rod, a driving auxiliary rod, a lifting rod, a lifting auxiliary rod, a leg placing plate, and a sliding plate. The driving auxiliary rod and lifting auxiliary rod ensure the stability of the leg lifting process and prevent failure of the driving and lifting rods during movement, thereby ensuring safety. The sliding plate is mounted on the outside of the leg placing plate using pulleys and sliding guide rails, allowing it to slide along the direction of the leg placing plate. This design accommodates individuals with varying leg lengths.

Based on the designed human leg lifting action mechanism, Creo 5.0 software was used to create a three-dimensional model of the entire mechanism, as shown in Figure 3.

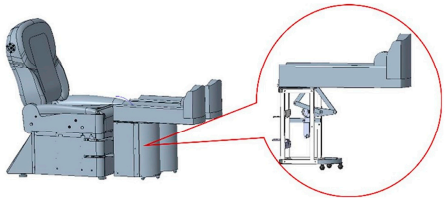

Figure 3. The 3D model of the mechanism.

A motion analysis aims to determine the trajectory, displacement, angular velocity, and angular acceleration of components, given the known mechanism dimensions and the motion law of the prime mover. The methods for a mechanism motion analysis include both graphical and analytical approaches. This paper investigates the motion characteristics of the leg lifting mechanism throughout its entire operation. Therefore, the analytical method

is employed to analyze the motion of key components—such as the driving rod, lifting rod, and leg placing plate—obtaining the motion parameter relationships between these components. Furthermore, ADAMS 2019 software is utilized to generate the motion curves of each component. The motion characteristics of the leg lifting mechanism are studied and observed.

The motion analysis of the leg lifting action mechanism designed in this paper is performed by first calculating the degrees of freedom of the mechanism [23]. It is known from the mechanical principle that the mechanism has a number of independent motion parameters that must be given when determining motion, which is called the degree of freedom of the mechanism [24], and the number is expressed by F. Its calculation formula is

$$F = 3n - (2P_l + P_h), \tag{1}$$

where F is the degree of freedom of the mechanism, n is the total component, P_l is the rotating or moving pair, and P_h is the higher pair.

As shown in Figure 3, the mechanism designed in this paper has a composite hinge composed of 3 components; then, there are 2 rotating pairs, the total components (n) is 5, the rotating pairs (P_l) are 7, and the higher pairs (P_h) are 0. According to Equation (1), the degree of freedom (F) of the mechanism is 1. Therefore, the leg lifting mechanism has 1 degree of freedom, meaning its motion is fully defined.

As shown in Figure 4, the driving rod of the key components of the leg lifting mechanism AB is $\vec{l_1}$, the lifting rod BC is $\vec{l_2}$, the leg placing plate DC is $\vec{l_3}$, and the fixing point AD is $\vec{l_4}$. The coordinate system as shown in the figure is established, with the X-axis forward as the starting point of the rotation angles θ_1, θ_2, and θ_3 of each component and the positive direction as the counterclockwise direction. Each component is expressed as a vector form, and the vector equation of the leg lifting mechanism can be obtained, namely

$$\vec{l_1} + \vec{l_2} = \vec{l_3} + \vec{l_4}. \tag{2}$$

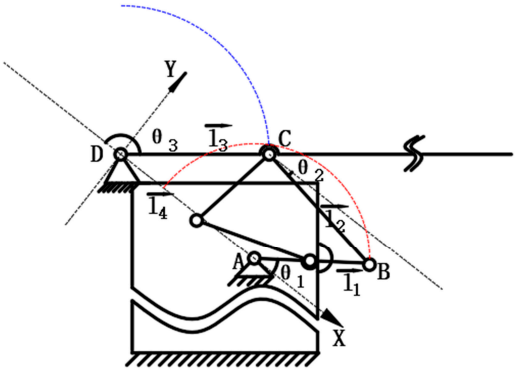

Figure 4. Kinematic analysis diagram of the mechanism.

(1) Location analysis

By writing the vector equation as a projection equation, we obtain

$$l_1 \cos\theta_1 + l_2 \cos\theta_2 = l_3 \cos\theta_3 + l_4, \tag{3}$$

$$l_1 \sin\theta_1 + l_2 \sin\theta_2 = l_3 \sin\theta_3, \tag{4}$$

It can be seen from Equations (3) and (4) that θ_2 and θ_3 are unknown quantities and the simultaneous equation can be solved:

$$\theta_3 = 2arctan\frac{P - \sqrt{P^2 + M^2 - N^2}}{M - N}, \tag{5}$$

where $P = 2l_1l_3sin\theta_1$, $M = 2l_3(l_1\cos\theta_1 - l_4)$, $N = {l_2}^2 - {l_1}^2 - {l_3}^2 - {l_4}^2 + 2l_1l_4\cos\theta_1$.

From θ_3 we obtain θ_2, namely

$$\theta_2 = arctan\frac{l_3sin\theta_3 - l_1sin\theta_1}{l_4 + l_3cos\theta_3 - l_1cos\theta_1}. \tag{6}$$

(2) Speed analysis

Take the derivative of Equations (3) and (4) with respect to time, and the velocity equation can be obtained:

$$\begin{cases} l_1\omega_1\cos\theta_1 + l_2\omega_2\cos\theta_2 = l_3\omega_3\cos\theta_3 + l_4 \\ l_1\omega_1\sin\theta_1 + l_2\omega_2\sin\theta_2 = l_3\omega_3\sin\theta_3 \end{cases}, \tag{7}$$

The angular velocities ω_2 and ω_3 can be obtained by solving the system of equations:

$$\omega_3 = \frac{\omega_1 l_1\sin(\theta_1 - \theta_2)}{l_3\sin(\theta_3 - \theta_2)}, \tag{8}$$

$$\omega_2 = \frac{-\omega_1 l_1\sin(\theta_1 - \theta_3)}{l_2\sin(\theta_2 - \theta_3)}. \tag{9}$$

(3) Acceleration analysis

Take the derivative of both sides of Equation (7) with respect to time, and the acceleration equation can be obtained:

$$\begin{cases} l_1{\omega_1}^2\cos\theta_1 + l_2a_2\sin\theta_2 + l_2{\omega_2}^2\cos\theta_2 = l_3a_3\sin\theta_3 + l_3{\omega_3}^2\cos\theta_3 \\ l_2a_2\cos\theta_2 - l_1{\omega_1}^2\sin\theta_1 - l_2{\omega_2}^2\sin\theta_2 = l_3a_3\cos\theta_3 - l_2{\omega_2}^2\sin\theta_3 \end{cases}, \tag{10}$$

The angular velocities a_2 and a_3 can be obtained by solving the system of equations:

$$a_3 = \frac{{\omega_1}^2 l_1\cos(\theta_1 - \theta_2) + l_2{\omega_2}^2 + l_3\omega_3 cos(\theta_3 - \theta_2)}{l_3\sin(\theta_3 - \theta_2)} \tag{11}$$

$$a_2 = \frac{-{\omega_1}^2 l_1\cos(\theta_1 - \theta_3) + l_3{\omega_3}^2 - l_2{\omega_2}^2 cos(\theta_2 - \theta_3)}{l_2\sin(\theta_2 - \theta_3)} \tag{12}$$

The angular displacement, angular velocity, and angular acceleration relationships between the driving rod, lifting rod, and leg placing plate can be derived from the motion analysis, thereby revealing the motion characteristics of the leg lifting mechanism.

2.1.3. Stage 3: Motion Analysis of Leg Lifting Action Mechanism Based on ADAMS

The CREO model data of the overall structure of the leg lifting action mechanism and the ADAMS model data are coupled and processed, the mechanism is reasonably simplified, the main motion mechanism of the leg lifting mechanism is retained, and the simplified motion model is shown in Figure 5.

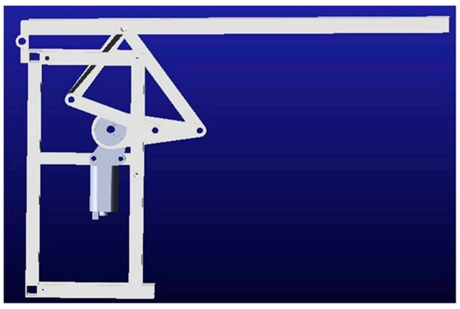

Figure 5. Motion model of the leg lifting action motion machine.

According to the characteristics and motion of the leg lifting action mechanism, the material properties and motion pairs of each component are defined in Tables 1 and 2.

Table 1. Material attribute table of parts.

Part Name	Model Drawing	Materials
Drive Rod	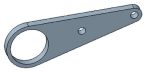	45 Steel
Lift Rod		45 Steel
Leg Placing Plate		Al6061 Alloy
Drive Auxiliary Rod		45 Steel
Lift Auxiliary Rod		45 Steel

Table 2. Parts and motion pair table.

Part Names	The Name of the Motion Pair	Number of Degrees of Freedom	Instructions
Motor	Fixed Pairs	0	Motor–Bracket
Drive Rod	Rotating Pairs	1	Drive Rod–Motor
Lift Rod	Rotating Pairs	1	Lift Rod–Drive Rod
Leg Placing Plate	Rotating Pairs	1	Leg Placing Plate–Lift Rod
Fixed Hinge	Fixed Pairs	0	Fixed Hinge–Bracket
Bracket	Fixed Pairs	0	Bracket–Earth
Moving Hinge	Rotating Pairs	1	Moving Hinge–Fixed Hinge
Drive Auxiliary Rod	Rotating Pairs	1	Drive Auxiliary Rod–Drive Rod
Lift Auxiliary Rod	Rotating Pairs	1	Lift Auxiliary Rod–Drive Auxiliary Rod
Lift Auxiliary Rod	Rotating Pairs	1	Lift Auxiliary Rod–Leg Placing Plate

The motor drive function is set by the step function, step (time, 0, 0, 10, 120 d) + step (time, 10, 0, 20, −120 d), which means that the 0~10 s motor drives the driving rod to rotate 120°, and the driving rod drives the lifting rod to drive the leg placing plate to lift 90°, that is, the lifting action process of the leg lifting mechanism. The 10~20 s motor drives the driving rod back to the initial position, where the leg placing plate falls to the initial position, that is, the leg lifting mechanism landing action process. This is the leg lifting mechanism lifting and landing a complete action. During the whole action process, the driving motor shows the motion law of accelerating first, then decelerating and finally stopping, as shown in Figure 6. To facilitate the study and observation of the motion characteristics of the leg lifting mechanism, the motor drive function is set to 5 cycles, that is, the leg lifting mechanism completes 5 lifting and landing actions.

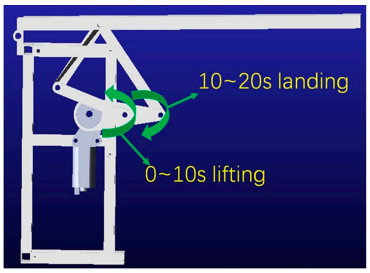

Figure 6. Schematic diagram of mechanism drive.

2.1.4. Stage 4: Strength Analysis of Leg Lifting Action Mechanism Based on ABAQUS

In this paper, Abaqus 2022 software is used to conduct a finite element analysis of the driving rod, lifting rod, and leg placing plate to verify the strength of the main components of the designed leg lifting action mechanism when it realizes the lift–landing action.

This section mainly analyzes the main components of the leg lifting mechanism. The model data of the leg lifting mechanism is imported into ABAQUS 2022 software, and the model is simplified at the same time, as shown in Figure 7.



Figure 7. The 3D model of lifting mechanism.

In the finite element analysis model of the leg lifting action mechanism, 45 steel was selected for the driving rod and lifting rod, and 6061 aluminum alloy was selected for the leg placing plate. The rest of the components are not analyzed, so the material properties are not described here [25]. The acceleration of gravity is g = 10 m/s^2. The main material parameters are shown in Table 3.

Table 3. Material parameters.

Materials	Density (kg·cm^{-3})	Elastic Modulus/MPa	Poisson's Ratio	Tensile Strength/MPa	Yield Strength/MPa
45 Steel	7.85	210,000	0.3	600	355
Al6061 Alloy	2.73	70,000	0.33	260	110

The mesh division should be based on the structural characteristics of the analysis object and practical problems to choose the appropriate element type. The finite element includes a solid element, shell element, beam element, volume element, and other element types. Since the analysis of the leg lifting mechanism has been simplified, and we hope to obtain a more real situation, the solid element is therefore used in this analysis. The unit type is C3D8R, an eight-node hexahedron linear reduction integral element. The mesh division of the mechanism is shown in Figure 8.

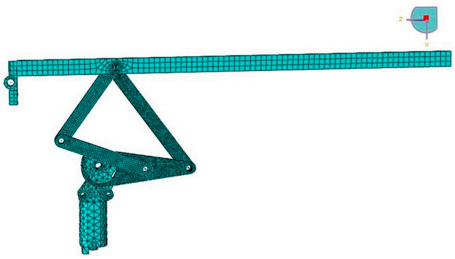

Figure 8. Lifting mechanism mesh model.

The total number of finite element model meshes of the leg lifting mechanism is 24,575. This analysis focuses on the analysis of the driving rod, lifting rod, and leg placing plate, so the element refinement is carried out. The finite element model meshes of the driving rod are 7950, the finite element model meshes of the lifting rod are 6180, and the finite element model meshes of the leg placing plate are 4215.

This section focuses on the analysis of the stress and strain behavior of the driving rod, lifting rod, and leg placing plate. To achieve this, fixed constraints were applied to both the motor and the lower hinge, which are treated as rigid bodies. The driving rod is connected to the motor and other components via hinge joints, ensuring that the only available component of relative motion (CORM) between the parts is a single rotational degree of freedom (UR1), with all other degrees of freedom constrained. A displacement of 2.1 radians was applied at the interface between the driving rod and the motor, enabling the leg lifting mechanism to execute the lifting motion. This setup allows for the investigation of the stress and strain distribution in the individual components during the leg lifting process.

Combined with the test results of force changes during the leg lifting action, the test results were set as the amplitude curve and applied to the front end of the leg placing plate. In the process of the leg lifting force experiment, it was found that the heel and the front end of the calf tend to press down during the leg lifting process. At the same time, the digital tension meter is also fixed at the front end of the leg. Therefore, in order to conform to the actual scene, the action range of the force is applied to the front end of the leg placement plate for about 200 mm. The application method is shown in Figure 9.

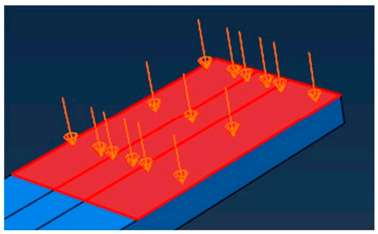

Figure 9. Method of force application.

2.2. Experiments

2.2.1. Experiments to Verify the Requirements for Human Leg Lifting Action

The test subjects were seated on designated chairs. During the experiment, the leg was fixed with soft rope and a wooden board, and the wooden board was firmly fixed at the lower end of the leg of the experimental object to prevent knee bending during the leg lifting process from affecting the test results. A digital tension meter was attached at the front end of the legs. During the process, the test operator holds the tension meter firmly while lifting the subjects' legs, ensuring that the tension meter remains perpendicular to the legs. An assistant uses a digital display protractor to measure the leg lifting angle, denoted as α, and records the test data. A schematic of the test setup is shown in Figure 10. In this study, a total of 20 volunteers participated in the experiment. The average age of the participants was 27.6 years old, and the standard deviation was 9.02. All participants

were healthy. The experiment was repeated at different times to ensure the reliability of the data. Specifically, each group of experiments carried out 3–5 repeated measurements in the early morning, before and after a lunch break, and before and after physical exercise, and between each experiment, 15–30 min of rest was arranged for the experimental subjects to ensure the accuracy and independence of each measurement data. Four groups of experimental models are shown in Figure 11.

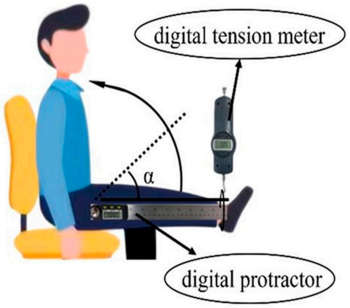

Figure 10. Schematic diagram of the lift test.



Figure 11. Four groups of test models.

Response surface methodology is a mathematical statistical method commonly used to find the best combination of tests under multi-factor conditions. It has the advantages of high accuracy, fewer tests, and lower cost [26]. In this paper, the BBD test method is used to establish a three-factor and three-level response regression model with human height A, body weight B, and human leg lifting angle C as factors to study the force of the human leg lifting process under various factors, and the test factors and levels are shown in Table 4.

Table 4. Experimental factors and levels.

Factors	Levels		
	−1	**0**	**1**
Height/cm	170	175	180
Weight/kg	70	80	90
Angle/deg	30	60	90

2.2.2. Experimental Verification of Device Prototype

Based on the motion analysis and strength analysis of the leg lifting mechanism, the physical prototype was made based on the structural model of the leg lifting device, and the physical prototype experiment was carried out. The experimental prototype is shown in Figure 12.

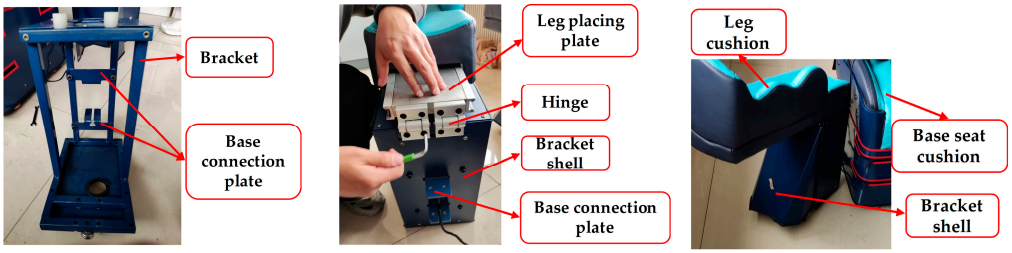

Figure 12. The experimental prototype.

The experimental model is shown in Figure 13, and the function of the leg lifting device was experimentally verified. The experimental process is as follows: the experimental subject sits on the experimental device, the legs are placed on the leg lifting device, the experimental auxiliary personnel controls the device to start and stop, and the experimental personnel carry out the leg stretching experiment. In the experimental verification part of the device prototype, it was still the original 20 experimental subjects. The average age of the experimental subjects was 27.6 years old, the standard deviation was 9.02, and the participants were healthy. Each experimental subject participated in the prototype experiment 3–5 times.

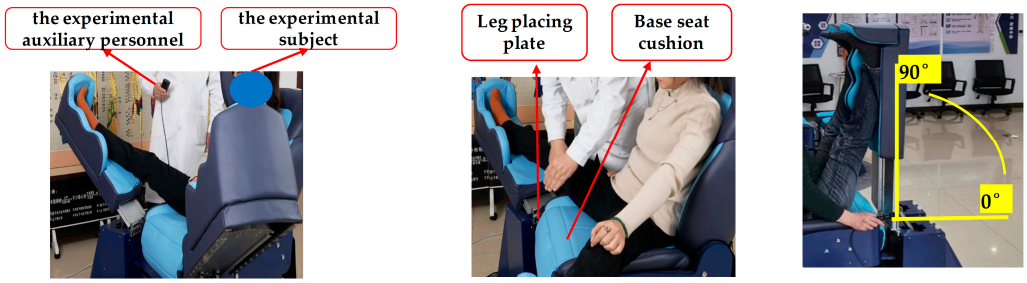

Figure 13. The experimental model.

We used a 5-level Likert scale questions to ask the subjects the following: (1) How do you feel about the stretching comfort of this leg lifting stretching device during use? A response of 1 is very uncomfortable, 2 is uncomfortable, 3 is general, 4 is comfortable, and 5 is very comfortable. (2) What do you think of the stretching effect of the device on your leg muscle group? A response of 1 is almost no effect, 2 is a little effect, 3 is medium effect, 4 is significant effect, and 5 is very significant. (3) In the process of using the leg lifting and stretching device, you feel how stable it is: 1 is very unstable, shaking violently; 2 is not very stable, shaking is more obvious; 3 is general, occasionally slight shaking; 4 is relatively stable, basically no shaking; 5 is very stable, no shaking. The feasibility of the leg lift device was verified through the subjective evaluation of the experimental subjects on the "stretching comfort", "muscle stretching effect", and "stability" of the leg lift device.

3. Results and Discussion

3.1. Results of the Requirements for Human Leg Lifting Action

During the leg lifting process, the leg force is recorded as F, and the unit is N. The response surface BBD test program and results are shown in Table 5. From Table 5, it can be seen that people with different heights and weights have less leg force when lifting 0–30°. As the lifting angle increases, the leg force becomes larger and larger. The response surface BBD test program and results are shown in Table 5.

Table 5. Test design scheme and results.

Serial Number	Height/cm	Weight/kg	Angle/deg	F/N
1	175~180	70~80	0~30	98.70
2	175~180	60~70	30~60	122.81
3	175~180	70~80	60~90	188.77
4	170~175	70~80	30~60	149.35
5	165~170	70~80	60~90	157.47
6	165~170	80~90	30~60	143.57
7	165~170	70~80	0~30	90.89
8	170~175	70~80	30~60	143.52
9	165~170	60~70	30~60	106.54
10	170~175	60~70	60~90	157.47
11	170~175	80~90	60~90	174.25
12	170~175	70~80	30~60	150.21
13	170~175	80~90	0~30	105.73
14	175~180	80~90	30~60	158.32
15	170~175	60~70	0~30	95.8

After performing significance tests on the linear function, second-order model, and third-order model and comparing the results of the model significance test, goodness-of-fit test, and correlation test, the second-order model was selected as the result of this experimental program. The regression model equation obtained using Design-Expert 13.0 software [27], with leg force as the response variable and human height (A), weight (B), and leg lifting angle (C) as independent variables, is shown in Equation (13). The results of the variance analysis of the regression model are shown in Table 6.

$$F = -9242.36292 + 99.68058A + 14.65079B - 5.23053C - 0.007600AB + 0.039150AC + 0.005708BC - 0.284767A^2 - 0.077642B^2 - 0.007352C^2. \quad (13)$$

Table 6. Analysis of variance for regression model equations.

Source	Sum of Squares	Mean Square	F-Value	*p*-Value	Distinctiveness
Model	12,776.71	1419.63	18.45	0.0025	Significant
A—Height	614.78	614.78	7.99	0.0368	
B—Weight	1231.32	1231.32	16.00	0.0103	
C—Angle	10,284.65	10,284.65	133.66	<0.0001	
AB	0.5776	0.5776	0.0075	0.9343	
AC	137.95	137.95	1.79	0.2382	
BC	11.73	11.73	0.1524	0.7123	
A^2	187.14	187.14	2.43	0.1796	
B^2	222.58	222.58	2.89	0.1497	
C^2	161.65	161.65	2.10	0.2069	
Lack of Fit	358.25	119.42	9.01	0.1015	Not Significant

As shown in Table 6, the *p*-value of 0.0025 ($p < 0.01$) for the model indicates that the regression model fits the data very well, demonstrating a significant fit. The influence of each factor on the model can be assessed by comparing the *p*-values and F-values presented in the table. The leg lifting angle (Factor C) has an extremely significant effect on the leg force, while both height (Factor A) and weight (Factor B) have significant effects on the leg force. The order of significance for the influence of each factor on the leg force is as follows: C > B > A > AC > BC > AB. Based on the regression model equation, the response surface and contour plots for the leg force were created to analyze the effects of the interaction between various factors. The results are shown in Figure 14.

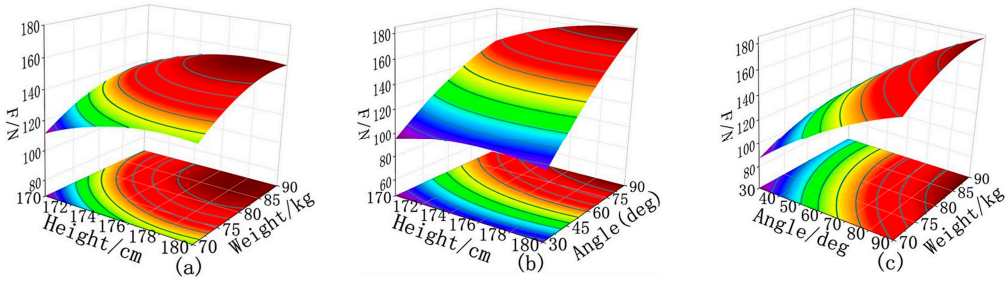

Figure 14. A 3D map and contour map of the response surface: (**a**) the effect of the interaction between height and weight on force; (**b**) the effect of the interaction between height and angle on force; (**c**) the effect of the interaction between angle and weight on force.

Using the response surface experimental data and software analysis, response surfaces and contour plots were created to visualize the interactions among various factors [28]. The results are shown in Figure 14. As shown in Figure 14a, the leg force increases with both height and weight. The weight curve is steeper than the height curve, indicating a stronger influence of weight on leg force. The response surface is steeper, and the contour lines are denser, suggesting a significant interaction between height and weight affecting leg force. As shown in Figure 14b, leg force increases with the lifting angle, while the change with height is minimal. The angle curve is steeper, indicating a stronger influence of the lifting angle on leg force. The response surface is steeper, and the contour lines are denser, highlighting a significant interaction between height and the angle of leg force. As shown in Figure 14c, leg force increases with both weight and angle. The angle curve is steeper than the weight curve, indicating that the angle has a greater impact on leg force. The response surface is steeper, and the contour lines are denser, suggesting a significant interaction between angle and weight on leg force.

The force change curve during the leg lifting action is shown in Figure 15. It is set as the amplitude curve and applied to the strength analysis model of the leg lifting mechanism shown in Figure 9.

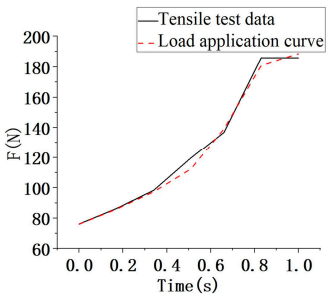

Figure 15. The force change curve.

3.2. Results of Leg Lifting Action Mechanism Based on ADAMS

In this paper, the simulation time was set to 100 s and the number of simulation steps was 1000. The mass center of position, angular velocity, and angular acceleration graphs of the driving rod, lifting rod, and leg placing plate were obtained at the end of the simulation, and the results are shown in Figures 16–18.

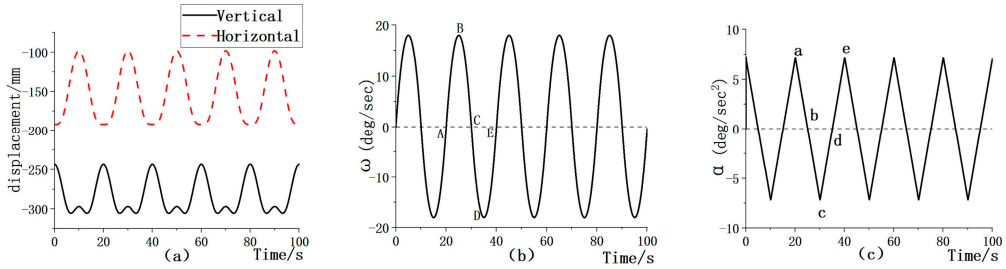

Figure 16. Motion simulation curve of the driving rod: (**a**) displacement curve; (**b**) angular velocity curve; (**c**) angular acceleration curve.

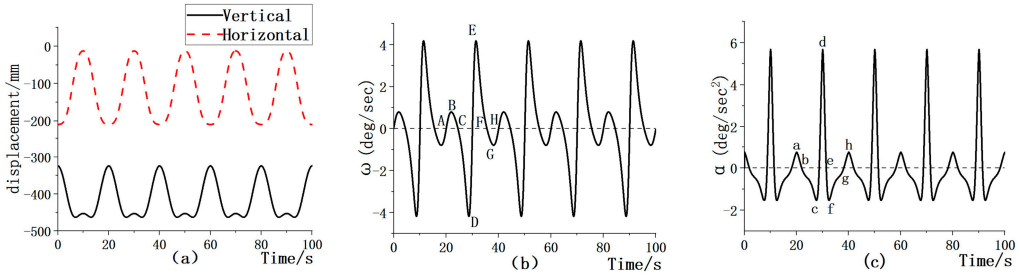

Figure 17. Motion simulation curve of the lifting rod: (**a**) displacement curve; (**b**) angular velocity curve; (**c**) angular acceleration curve.

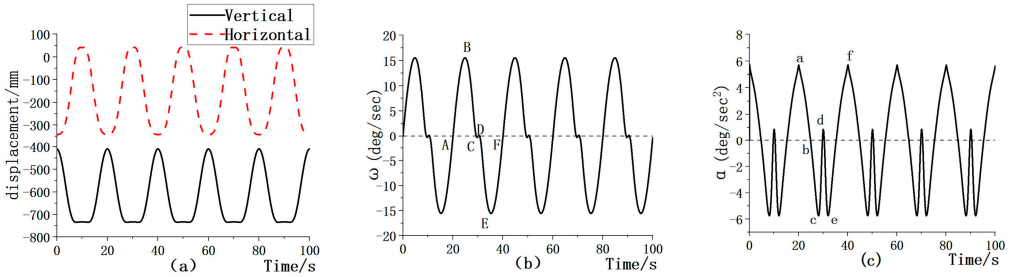

Figure 18. Motion simulation curve of leg placing plate: (**a**) displacement curve; (**b**) angular velocity curve; (**c**) angular acceleration curve.

As shown in Figure 16a, the peak displacement of the center of mass of the driving rod in the vertical and horizontal directions differs from the initial value by approximately 62 mm and 94 mm, respectively. This indicates that the motion range of the driving rod meets the design requirements of the lifting mechanism. A–E in Figure 16b represent the variation in the angular velocity of the driving rod during a complete lifting and landing cycle. The maximum angular velocity is 18.01 deg/s, and the angular velocity change process is relatively stable. Additionally, a–e in Figure 16c illustrate the variation in the angular acceleration of the driving rod during the full lifting and landing cycle. The maximum angular acceleration is 7.21 deg/s^2, and the change process of angular acceleration is relatively stable. By analyzing the displacement, angular velocity, and angular acceleration curves of the driving rod in Figure 16, it is evident that the motion performance of the driving rod is satisfactory and meets the design specifications [29].

As shown in Figure 17a, the peak displacement of the center of mass of the lifting rod in the vertical and horizontal directions differs from the initial value by approximately 138 mm and 197 mm, respectively. This indicates that the motion range of the lifting rod meets the design requirements of the lifting mechanism. A–H in Figure 17b represent the variation in the angular velocity of the lifting rod during a complete lifting and landing cycle. The maximum angular velocity is 4.18 deg/s, and the angular velocity change process is relatively stable. Additionally, a–h in Figure 17c illustrate the variation in the angular

acceleration of the lifting rod during the full lifting and landing cycle. The maximum angular acceleration is 5.68 deg/s^2, and the change process of angular acceleration is relatively stable. By analyzing the displacement, angular velocity, and angular acceleration curves of the lifting rod in Figure 17, it is evident that the motion performance of the lifting rod is satisfactory and meets the design specifications.

As shown in Figure 18a, the peak displacement of the center of mass of the leg placing plate in the vertical and horizontal directions differs from the initial value by approximately 324 mm and 300 mm, respectively. This indicates that the motion range of the leg placing plate meets the design specifications of the lifting mechanism. A–F in Figure 18b represent the variation in the angular velocity of the leg placing plate during a complete lifting and landing cycle. The maximum angular velocity is 15.55 deg/s, and the angular velocity change process is relatively stable. Additionally, a–f in Figure 18c illustrate the variation in the angular acceleration of the leg placing plate during the complete lifting and landing cycle. The maximum angular acceleration is 5.76 deg/s^2, and the change process of angular acceleration is relatively stable. By analyzing the displacement, angular velocity, and angular acceleration curves of the leg placing plate in Figure 18, it can be concluded that the motion performance is satisfactory and meets the design specifications.

3.3. Results of Leg Lifting Action Mechanism Based on ABAQUS

The simulation results of the driving rod are shown in Figure 19. From the equivalent stress cloud diagram and strain cloud diagram, it can be seen that the maximum stress of the driving rod under this force condition is 102.5 MPa and the maximum strain is 5.091 $\times$ 10^{-4} mm. According to the GB/T 699-2015 standard [30], the tensile strength of 45 steel is 600 MPa and the yield strength is 355 MPa, while the maximum stress of the driving rod is less than the yield strength of 45 steel, so the strength and stiffness of the driving rod meet the design requirements.

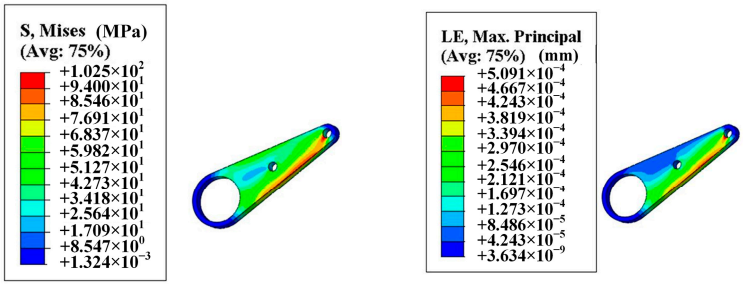

(**a**) (**b**)

Figure 19. Stress–strain cloud diagram of the driving rod: (**a**) stress cloud diagram; (**b**) strain cloud diagram.

The simulation results of the lifting rod are shown in Figure 20. According to the equivalent stress cloud diagram and strain cloud diagram, it can be seen that the maximum stress of the lifting rod under this force condition is 88.12 MPa and the maximum strain is 2.066 $\times$ 10^{-4} mm. According to the GB/T 699-2015 standard, the tensile strength of 45 steel is 600 MPa and the yield strength is 355 MPa, while the maximum stress of the lifting rod is less than the yield strength of 45 steel, so the strength and stiffness of the lifting rod meet the design requirements.

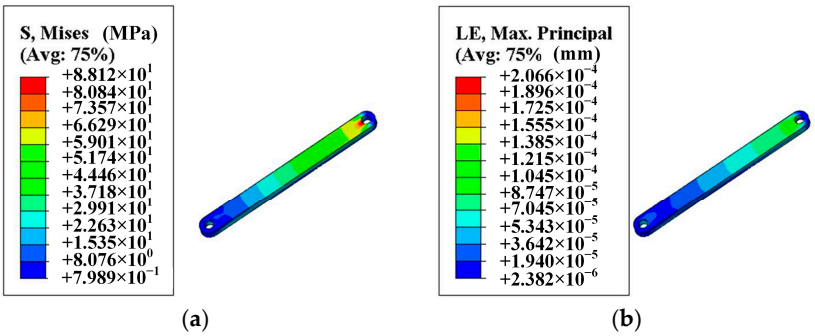

Figure 20. Stress–strain cloud diagram of lifting rod: (**a**) stress cloud diagram; (**b**) strain cloud diagram.

The simulation results of the leg placing plate are shown in Figure 21. According to the equivalent stress cloud diagram and strain cloud diagram, it can be seen that the maximum stress of the leg placing plate under this force condition is 40.5 MPa and the maximum strain is 5.4×10^{-4} mm. According to the GB/T 3191-2019 standard [31], the tensile strength of 6061 aluminum alloy is 260 MPa, and the maximum stress of the leg placing plate is less than the tensile strength of 6061 aluminum alloy, so the strength and stiffness of the leg placing plate meet the design requirements.

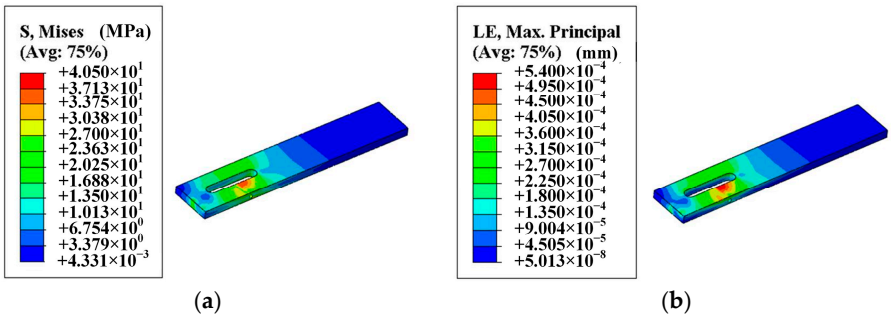

Figure 21. Stress–strain cloud diagram of leg placing plate: (**a**) stress cloud diagram; (**b**) strain cloud diagram.

3.4. Results of the Device Prototype

The experimental results show that the lifting angle of the leg lifting device ranges from 0° to 90°, which can meet the design requirements. The subjective evaluation results of the experimental subjects on the "stretching comfort", "muscle stretching effect", and "stability" of the leg lift device are shown in Figure 22. In terms of "stretching comfort", a total of 14 people chose level 4 "comfortable" and level 5 "very comfortable", reflecting the higher comfort of the leg lifting device during the stretching process, of which 6 people rated it lower. The reason is that the subjects feel that the muscle is stretched more obviously during the leg stretching process, so they feel uncomfortable. In terms of the "muscle stretching effect", only one person felt "almost no effect". Combined with comfort evaluation, it can be seen that the leg lifting device can give a good leg stretching effect. In terms of "stability", there was no choice for level 1 "very unstable, shaking violently", and there were 17 people in level 4 and level 5. Therefore, the leg lifting device has good stability and no safety hazard when performing leg stretching. In summary, the leg lifting device achieved a high evaluation in the three aspects of "stretching comfort", "muscle stretching effect", and "stability", which verifies the feasibility of the leg lifting device design.

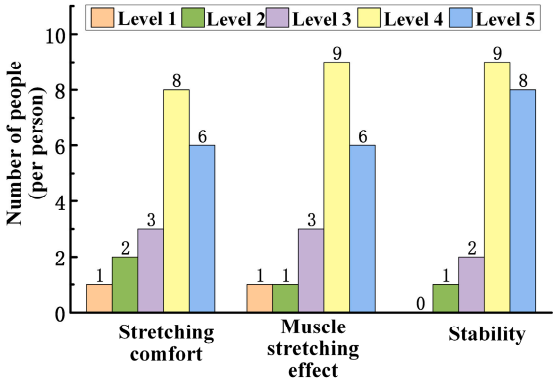

Figure 22. The experimental results.

4. Conclusions

(1) Based on the BBD response surface method, the experimental results of the force change of the human leg during the lifting action show that the leg lifting angle has the most significant effect on the leg force. Under different height and weight conditions, the leg force is small when the leg lifting angle is 0–30°. As the lifting angle increases, the leg force also increases, and the maximum is at 90°, which guides the design of the leg lifting mechanism and the establishment of the model.

(2) The human leg lifting mechanism was modeled using CREO, and the displacement equation, angular velocity equation, and angular acceleration equation of the mechanism were derived through a motion analysis and calculation of the mechanism. The simulation curves of the mechanism derived from ADAMS show that the motion process of the leg lifting mechanism is relatively smooth and the motion position meets the actual demand of leg extension.

(3) Combined with the test results of the force changes during the leg lifting action, the strength of the key components during the movement of the mechanism was obtained through ABAQUS, and the results show that the maximum stress of the driving rod during the lifting process is 102.5 MPa, the maximum stress of the lifting rod is 88.12 MPa, and the maximum stress of the leg placing plate is 40.5 MPa, which are less than the material strength requirements, so the strength of the leg lifting mechanism meets the design requirements.

(4) A prototype of the device was made and experimentally validated with leg lifting. The experimental results show that the lifting angle of the leg lifting device ranges from 0° to 90°, which can meet the design requirements. In the process of stretching, the comfort and stability are good, and the muscle has an obvious stretching effect.

In this paper, a leg lifting stretching device was designed based on the force of human leg lifting action, and the influencing factors of leg force in the process of human leg lifting were explored. The mechanism was analyzed based on the leg force to verify the feasibility of the leg lifting device. In future research, the structure of the leg lifting device will continue to be optimized, and the strength of the mechanism will be further analyzed and studied, for example, a strength analysis of the connecting pins. The control strategy of this study is not clear enough. In the future, the control method of the proposal will be studied in depth to achieve a better leg stretching effect.

Author Contributions: Conceptualization, R.G.; data curation, J.G. and S.Z.; funding acquisition, R.G.; methodology, J.G.; project administration, R.G.; software, J.G. and S.Z.; supervision, R.G.; validation, S.Z.; visualization, H.X.; writing—original draft, J.G.; writing—review and editing, S.Z. and H.X. All authors have read and agreed to the published version of the manuscript.

Funding: This work was supported by a grant from the Longmen Laboratory Project (grant numbers LMQYTSKT036).

Institutional Review Board Statement: The study was conducted following local legislation: the Measures for Ethical Review of Life Science and Medical Research Involving Human Beings (https://www.gov.cn/zhengce/zhengceku/2023-02/28/content_5743658.htm (accessed on 16 January 2025)).

Informed Consent Statement: Informed consent was obtained from all the subjects involved in the study.

Data Availability Statement: All the test data mentioned in this paper will be made available upon request to the corresponding author with appropriate justification.

Conflicts of Interest: The authors declare no conflicts of interest.

References

1. Pega, F.; Náfrádi, B.; Momen, N.C.; Ujita, Y.; Streicher, K.N.; Prüss-Üstün, A.M.; Descatha, A.; Driscoll, T.; Fischer, F.M.; Godderis, L.; et al. Global, Regional, and National Burdens of Ischemic Heart Disease and Stroke Attributable to Exposure to Long Working Hours for 194 Countries, 2000–2016: A Systematic Analysis from the WHO/ILO Joint Estimates of the Work-Related Burden of Disease and Injury. *Environ. Int.* **2021**, *154*, 106595. [CrossRef] [PubMed]
2. Qassim, H.M.; Wan Hasan, W.Z. A Review on Upper Limb Rehabilitation Robots. *Appl. Sci.* **2020**, *10*, 6976. [CrossRef]
3. Ning, Y.; Wang, H.; Liu, Y.; Wang, Q.; Rong, Y.; Niu, J. Design and Analysis of a Compatible Exoskeleton Rehabilitation Robot System Based on Upper Limb Movement Mechanism. *Med. Biol. Eng. Comput.* **2024**, *62*, 883–899. [CrossRef]
4. Kwakkel, G.; Kollen, B.J.; Krebs, H.I. Effects of Robot-Assisted Therapy on Upper Limb Recovery after Stroke: A Systematic Review. *Neurorehabil. Neural Repair.* **2008**, *22*, 111–121. [CrossRef]
5. Lu, J.; Chen, Z.; Wu, H.; Yang, W.; Chen, H. Effect of lower limb rehabilitation robot on lower limb motor function of hemiplegic patients after stroke. *Chin. J. Contemp. Neurol. Neurosurg.* **2017**, *17*, 334–339. [CrossRef]
6. Talaty, M.; Esquenazi, A.; Briceno, J.E. Differentiating Ability in Users of the ReWalk^{TM} Powered Exoskeleton: An Analysis of Walking Kinematics. In Proceedings of the 2013 IEEE 13th International Conference on Rehabilitation Robotics (ICORR), Seattle, WA, USA, 24–26 June 2013; pp. 1–5.
7. Neuhaus, P.D.; Noorden, J.H.; Craig, T.J.; Torres, T.; Kirschbaum, J.; Pratt, J.E. Design and Evaluation of Mina: A Robotic Orthosis for Paraplegics. In Proceedings of the 2011 IEEE International Conference on Rehabilitation Robotics, Zurich, Switzerland, 29 June–1 July 2011; pp. 1–8.
8. Li, Z.; Ren, Z.; Zhao, K.; Deng, C.; Feng, Y. Human-Cooperative Control Design of a Walking Exoskeleton for Body Weight Support. *IEEE Trans. Ind. Inform.* **2020**, *16*, 2985–2996. [CrossRef]
9. Chen, Q. Design, Analysis and Experimental Study of a Cable-Driven Parallel Waist Rehabilitation Robot. *J. Mech. Eng.* **2018**, *54*, 126. [CrossRef]
10. Zimmermann, Y.; Sommerhalder, M.; Wolf, P.; Riener, R.; Hutter, M. ANYexo 2.0: A Fully Actuated Upper-Limb Exoskeleton for Manipulation and Joint-Oriented Training in All Stages of Rehabilitation. *IEEE Trans. Robot.* **2023**, *39*, 2131–2150. [CrossRef]
11. Pang, Z.; Wang, T.; Wang, Z.; Yu, J.; Sun, Z.; Liu, S. Design and Analysis of a Wearable Upper Limb Rehabilitation Robot with Characteristics of Tension Mechanism. *Appl. Sci.* **2020**, *10*, 2101. [CrossRef]
12. Yan, H.; Wang, H.; Chen, P.; Niu, J.; Ning, Y.; Li, S.; Wang, X. Configuration Design of an Upper Limb Rehabilitation Robot with a Generalized Shoulder Joint. *Appl. Sci.* **2021**, *11*, 2080. [CrossRef]
13. Fang, B.; Shen, L.; Li, Y.; Zhang, Y. Research of coordinated control for gait rehabilitation training robot. *J. Mech. Electr. Eng.* **2010**, *27*, 106–110. [CrossRef]
14. Zou, Y.; Wang, N.; Wang, X.; Ma, H.; Liu, K. Design and Experimental Research of Movable Cable-Driven Lower Limb Rehabilitation Robot. *IEEE Access* **2019**, *7*, 2315–2326. [CrossRef]
15. Kumar, S.; Wöhrle, H.; Trampler, M.; Simnofske, M.; Peters, H.; Mallwitz, M.; Kirchner, E.A.; Kirchner, F. Modular Design and Decentralized Control of the Recupera Exoskeleton for Stroke Rehabilitation. *Appl. Sci.* **2019**, *9*, 626. [CrossRef]
16. Shi, X. Design & Analysis of the Mechanical System for a Spacial 4-DOF Series-Parallel Hybrid Lower Limb Rehabilitation Robot. *J. Mech. Eng.* **2017**, *53*, 48. [CrossRef]

17. Ceccarelli, M.; Sanz, S.; Díaz, V.; Russo, M. Design and Construction of a Prototype of an Assisting Device for Arm Exercise. *Machines* **2024**, *12*, 145. [CrossRef]
18. Jeon, K.-W.; Chung, H.-J.; Jung, E.-J.; Kang, J.-S.; Son, S.-E.; Yi, H. Development of Shoulder Muscle-Assistive Wearable Device for Work in Unstructured Postures. *Machines* **2023**, *11*, 258. [CrossRef]
19. Russo, M.; Ceccarelli, M. Analysis of a Wearable Robotic System for Ankle Rehabilitation. *Machines* **2020**, *8*, 48. [CrossRef]
20. Herrera-Valenzuela, D.; Díaz-Peña, L.; Redondo-Galán, C.; Arroyo, M.J.; Cascante-Gutiérrez, L.; Gil-Agudo, Á.; Moreno, J.C.; del-Ama, A.J. A Qualitative Study to Elicit User Requirements for Lower Limb Wearable Exoskeletons for Gait Rehabilitation in Spinal Cord Injury. *J. NeuroEng. Rehabil.* **2023**, *20*, 138. [CrossRef]
21. Cho, D.Y.; Park, S.-W.; Lee, M.J.; Park, D.S.; Kim, E.J. Effects of Robot-Assisted Gait Training on the Balance and Gait of Chronic Stroke Patients: Focus on Dependent Ambulators. *J. Phys. Ther. Sci.* **2015**, *27*, 3053–3057. [CrossRef]
22. Hassan, M.; Kadone, H.; Suzuki, K.; Sankai, Y. Wearable Gait Measurement System with an Instrumented Cane for Exoskeleton Control. *Sensors* **2014**, *14*, 1705–1722. [CrossRef]
23. Zeng, D.; Jing, G.; Su, Y.; Wang, Y.; Hou, Y. A Novel Decoupled Parallel Mechanism with Two Translational and One Rotational Degree of Freedom and Its Performance Indices Analysis. *Adv. Mech. Eng.* **2016**, *8*, 1687814016646936. [CrossRef]
24. Hu, J.; Sun, Y.; Cheng, Y. High Mechanical Advantage Design of Six-Bar Stephenson Mechanism for Servo Mechanical Presses. *Adv. Mech. Eng.* **2016**, *8*, 1687814016656108. [CrossRef]
25. Menzemer, C.; Hilty, E.; Morrison, S.; Minor, R.; Srivatsan, T. Influence of Post Weld Heat Treatment on Strength of Three Aluminum Alloys Used in Light Poles. *Metals* **2016**, *6*, 52. [CrossRef]
26. Jin, Y.; Gu, Q.; Liu, S.; Yang, C. Experimental Investigation and Modeling of Force-Induced Surface Errors for the Robot-Assisted Milling Process. *Machines* **2023**, *11*, 655. [CrossRef]
27. Wen, S.; She, R.; Zhao, Z.; Gong, Y. Optimization of Motor Rotor Punch Wear Parameters Based on Response Surface Method. *Machines* **2024**, *12*, 671. [CrossRef]
28. Lu, K.; Yin, C.; Qian, J.; Sun, Z.; Wang, L. Parameter Optimization Method for Centrifugal Feed Disc Discharging Based on Numerical Simulation and Response Surface. *Machines* **2024**, *12*, 799. [CrossRef]
29. Essomba, T.; Phu, S.N. Kinematic Design of a Hybrid Planar-Tripod Mechanism for Bone Reduction Surgery. *Mech. Ind.* **2020**, *21*, 403. [CrossRef]
30. *GB/T 699-2015*; Quality Carbon Structure Steels. SAC: Beijing, China, 2015.
31. *GB/T 3191-2019*; Extrusion Rods and Bars of Aluminium and Aluminium Alloys. SAC: Beijing, China, 2019.

Disclaimer/Publisher's Note: The statements, opinions and data contained in all publications are solely those of the individual author(s) and contributor(s) and not of MDPI and/or the editor(s). MDPI and/or the editor(s) disclaim responsibility for any injury to people or property resulting from any ideas, methods, instructions or products referred to in the content.